

The Combination of Black Hat Transform and U-Net in Image Enhancement and Blood Vessel Segmentation in Retinal Images

Cahyo Pambudi Darmo^{1*}, Lucky Indra Kesuma², Dite Geovani³

¹Department of Informatics, Faculty of Computer Science, Universitas Sjakhyakirti

²Department of Information System, Faculty of Computer Science, Universitas Sjakhyakirti

³Department of Mathematics, Faculty of Mathematics and Natural Sciences, Universitas Sriwijaya

*cahyopambudi@unisti.ac.id

ABSTRACT

Diabetic Retinopathy (DR) is a disorder of the eye caused by damage to blood vessels in the retina. Damage to the retinal blood vessels can be analyzed by segmenting the blood vessels on the image. This study proposes a combination of image enhancement and blood vessel segmentation in retinal images. Retinal image enhancement is carried out using the black hat transform method to obtain a detailed view of blood vessels in retinal images. Segmentation of blood vessels in retinal images is carried out using the U-Net architecture. The results of image enhancement are measured using MSE and PSNR. This study has an MSE value below 0.05 and a PSNR above 90dB. The MSE and PSNR values obtained show that the black hat transform method is very good at image enhancement. Segmentation has an accuracy value above 0.95 and a sensitivity value above 0.85. In addition, the specificity value and f1-score are above 0.8. This shows that the proposed stages of image enhancement and blood vessel segmentation are able to accurately recognize blood vessel features in retinal images.

Keywords: Retinal, Blood vessels, black hat transform, segmentation, U-Net

1. INTRODUCTION

The eye is a very important organ for humans that functions as a sensitive sense of sight. Abnormalities in the eye will interfere with humans in carrying out their daily lives [1]. An eye disorder that causes loss of vision in humans is Diabetic Retinopathy (DR) [2]. DR is a disorder of the eye caused by damage to blood vessels in the retina [3]. Damage to blood vessels in the retina can be analyzed by segmenting blood vessels on retinal images that have been taken with a fundus camera [4]. Segmentation of the retinal blood vessels is an appropriate way to separate the blood vessels from the retinal image [5]. Segmentation that is done manually takes a long time and is subjective, and prone to errors, so it is necessary to develop an automatic segmentation algorithm to perform segmentation [6]–[8].

Convolutional Neural Network (CNN) is a popular and widely used method for performing automatic segmentation [9]. A CNN architecture that is frequently used in biomedical image segmentation is the U-Net architecture [10]. The U-Net architecture has two parts, namely encoder and decoder. The encoder section functions to extract features from the image while the decoder functions to perform image feature reconstruction [11]. The process of the encoder part works to reduce the size of the

Cahyo Pambudi Darmo, Lucky Indra Kesuma, Dite Geovani
The Combination of Black Hat Transform and U-Net in Image Enhancement and
Blood Vessel Segmentation in Retinal Images

input matrix by increasing the number of feature maps and the decoder part works to return the size of the matrix to its original size by minimizing the number of feature maps [9]. Several studies using the U-Net architecture have been carried out. Fu *et al.* [12] performed blood vessel segmentation using the U-Net architecture with performance results of accuracy above 90% and sensitivity below 75%, but did not measure specificity and f1-score. Venkatesh *et al.* [13] performed skin cancer segmentation using the U-Net architecture with results of performance accuracy above 90%, but did not measure the value of sensitivity, specificity, and f1-score. Saood *et al.* [14] performed lung segmentation using the U-Net architecture with results of accuracy, sensitivity, and specificity above 90%, but did not measure the f1-score. Research conducted by Fu *et al.* [12], Venkatesh *et al.* [13], and Saood *et al.* [14] did not perform image enhancement prior segmentation.

Image enhancement needs to be done before performing image segmentation so that good image quality is able to provide precise and accurate segmentation results [15]. Image segmentation results are influenced by image quality [16]. In general, retinal images have low quality due to dark image intensity, noise, and varying blood vessel sizes [17]. In addition, retinal images also have low noise and contrast between the blood vessels and the image background [18]. Improving retinal image quality is important to obtain stable retinal image contrast and improve image quality [5], [19]. An image enhancement method that can improve image quality is black hat transform [20], [21]. Black hat transform is an image enhancement method that is able to highlight a part without causing noise in the image [22]. Black hat transform is able to enhance the appearance of dark areas of the image in detail [23]. Several studies using the black hat transform method have been carried out. Kushol *et al.* [24] applied black hat transform to improve image quality in segmenting blood vessels and obtaining accuracy values above 90%. Mughal *et al.* [25] applied black hat transform to improve image quality in classifying breast cancer and obtained accuracy and specificity above 90%. Yadav [26] applied black hat transform to improve image quality in exudate segmentation by obtaining accuracy, sensitivity, and specificity values above 95%.

In this study, two stages were proposed in the detection of Diabetic Retinopathy (DR), which consisted of image enhancement stages and retinal image blood vessel segmentation. Image enhancement is carried out using the black hat transform method with the aim of eliminating noise in the image and displaying the detailed structure of blood vessels from retinal images. Segmentation of blood vessels in retinal images is carried out using the U-Net architecture to extract blood vessel features from retinal images. The success rate of the black hat transformation method for image enhancement is measured by calculating the MSE and PSNR values. The success rate of the U-Net architecture for segmenting blood vessels in retinal images is measured by calculating the accuracy, sensitivity, specificity, and f1 scores. The stages proposed in this study are expected to help the work of medical experts to detect Diabetic Retinopathy (DR).

2. MATERIAL AND METHODS

In this study consisted of several stages, namely description of retinal image data, image enhancement, segmentation of blood vessels with U-Net architecture, and evaluation of results. The flowchart of the method in this study can be seen in Figure 1.

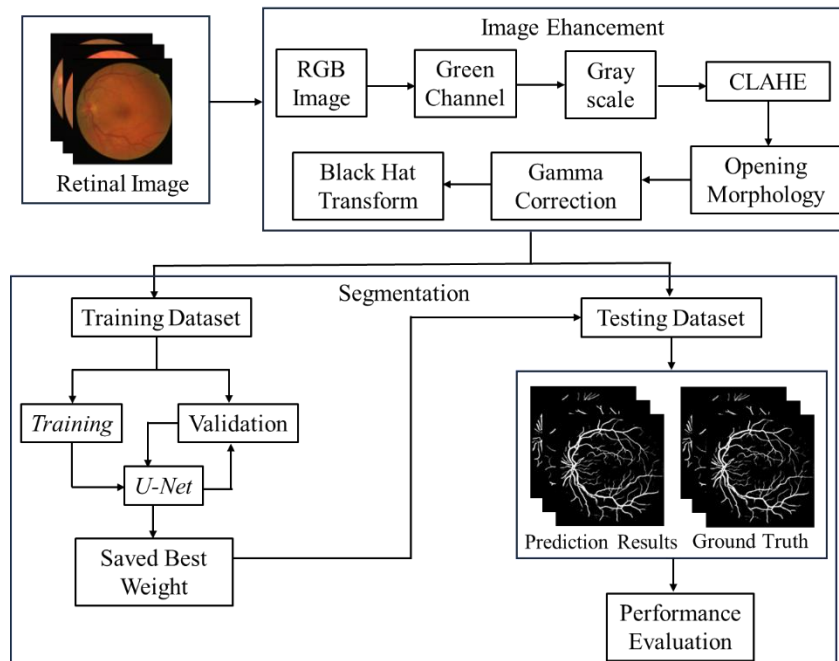

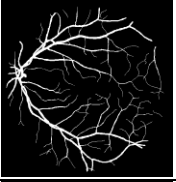



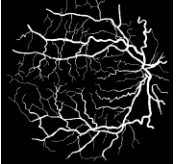

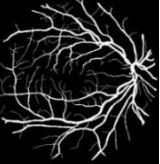


FIGURE 1. Proposed Method

2.1 DATA DESCRIPTION

The dataset used in this study is the Digital Images for Vessel Extraction (DRIVE) dataset. The DRIVE dataset can be obtained at <https://www.isi.uu.nl/Research/Databases/DRIVE/>. The DRIVE dataset is a retinal image dataset that is widely used in several studies and can be accessed free of charge. The DRIVE dataset consists of 40 retinal image samples taken randomly from 400 diabetes patients aged 25 to 90 years in the Netherlands. This dataset is divided into two, namely 20 training images and 20 testing images. The DRIVE dataset also contains analysis results from eye specialists which are used as ground truth. Some displays of training and test image data on the DRIVE dataset can be seen in Table 1.

TABLE 1.
Training and Test Data on the DRIVE Dataset

No	Training Data		Test Data			
	Name File	Retinal Images	Ground Truth	Name File	Retinal Images	Ground Truth
1	21_training.tif			01_test.tif		
2	22_training.tif			02_test.tif		

2.2 IMAGE ENHANCEMENT

Image enhancement stages are carried out to improve the quality of the image used. The image improvement process carried out in this study is as follows.

2.2.1 GREEN CHANNEL

In the first stage, a BGR (Blu Green Red) image is changed to RGB (Red Green Blue), then a split is performed on the image channel to retrieve the green channel from the retina image. The green channel was taken because the appearance of the blood vessels is clearer in the green channel [16].

2.2.2 GRAYSCALE

In the grayscale stage, the green channel image is converted to a grayscale or gray image. Grayscale has a range of color gradations between black and white which is very appropriate for image processing [16]. Image conversion to grayscale is performed to clarify contrast variations in the image [27]. This grayscale process can be described by the Equation (1) [28].

$$l = (R * 0.299 + (g * 0.587) + (b * 0.114)) \quad (1)$$

where, l is a grayscale value with the range 1 – 256, R is red channel value, G is green channel value, and B is blue channel value.

2.2.3 CONTRAST LIMITED ADAPTIVE HISTOGRAM EQUALIZATION (CLAHE)

The CLAHE method is used to display the hidden features of the image by applying a histogram equalization for each pixel value. CLAHE works by providing a maximum height limit value of a histogram (clip limit). Clip limit is used to divide the image into several small parts with identical sizes so that the histogram of the output image matches the histogram shown by the distribution parameters [29]. The clip limit calculation process uses Equation (2) [16].

$$b = \frac{k}{l} \left(1 + \frac{\alpha}{100} (s_{max} - 1) \right) \quad (2)$$

where, b is the clip limit value, k is the area size of the region, l is a grayscale value with the range 1 – 256, and α is the clip factor with the range 0 – 100.

2.2.4 OPENING MORPHOLOGY

The opening morphology is used to improve the quality and smooth the appearance of the image surface and make the appearance of objects in the image clearer. The morphological opening operation is a combination of erosion and dilation

processes [30]. The operating process of opening morphology is defined using Equations (3), (4), and (45) [31].

$$A \circ B = (A \ominus B) \oplus B \quad (3)$$

$$A \ominus B = \{x | (B)_x \cap A^c \neq \emptyset\} \quad (4)$$

$$A \oplus B = \{x | (B)_x \cap A \neq \emptyset\} \quad (5)$$

where, A is the original image pixel matrix, A^c is the complement of the original image pixel matrix, and B is a structuring element in the form of an operator matrix in the form of lines, disks, diamonds, and others. \circ is the opening morphology operation, \ominus is the erosion operation, and \oplus is the dilation operation.

2.2.5 GAMMA CORRECTION

Gamma correction aims to increase image contrast [32]. Gamma correction is a nonlinear operation that is used as a function of intensity transformation [33]. The gamma correction operation is defined using Equation (6) [32].

$$I_{gam}(x, y) = I(x, y)^\gamma \quad (6)$$

for $x = 1, 2, \dots, m$ and $y = 1, 2, \dots, n$, where $I(x, y)$ is the image pixel value at position (x, y) , m is the number of rows of the image pixel matrix, n is the number of image pixel matrix columns, γ is the gamma value, and $I_{gam}(x, y)$ is the result of the intensity of gamma correction.

2.2.6 BLACK HAT TRANSFORM

Black hat transform is used to enhance the appearance of dark areas of the image in detail without causing noise in the image. Black hat transform works by displaying dark objects in an image with a light background. The black hat transform process uses the closing operation. The closing operation removes the small holes in the center of the image and connects adjacent pixels to refine the features in the image [16]. The black hat transform operation is defined using Equations (7) and (8) [24].

$$A_{bot} = (A \bullet B) - A \quad (7)$$

$$A \bullet B = (A \oplus B) \ominus B \quad (8)$$

where, A is the original image pixel matrix, B is a structuring element in the form of an operator matrix in the form of lines, disks, diamonds, and others. A_{bot} is the result of black hat transform and \bullet is closing operation.

2.3 SEGMENTATION: U-NET ARCHITECTURE

After the image enhancement stage, a patching technique is carried out to increase the training data where the resulting image from the black hat transform is divided into small pieces and then segmented on the retinal image. Segmentation is performed to separate the vascular features from the retinal image. The segmentation stage is carried out using the U-Net architecture. The U-Net architecture consists of two parts, namely the decoder and encoder. The encoder part functions to extract useful features from the input image and the decoder is used to reconstruct the features to get the final segmentation results. The encoder has a convolution layer process, ReLU activation function, batch normalization, and maxpooling. The U-Net architecture used at the segmentation stage can be seen in Figure 2.

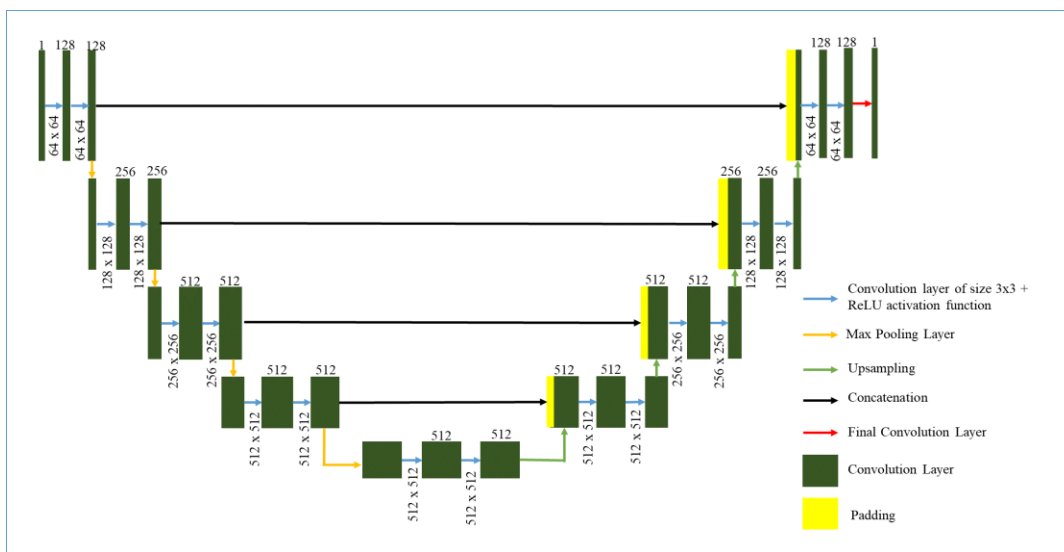


FIGURE 2. U-Net Architecture for Optic Disc and Optic Cup Segmentation

The convolution layer aims to learn the feature representation of the input. This layer consists of a set of convolutional kernels for extracting local features from inputs [34]. The process of calculating the convolution operation on the convolutional layer uses Equation (9).

$$v_{i,j} = \left(\sum_{u=0}^{n-1} \sum_{v=0}^{n-1} a_{u+i,v+j} \times k_{u+1,v+1} \right) + b_q \quad (9)$$

for $i = 1, 2, \dots, n$ and $j = 1, 2, \dots, n$, where $v_{i,j}$ is the convolution matrix entry in the baris i -th row, j -th column, $a_{u+i,v+j}$ is the input matrix entry $u + i$ -row, $v + j$ -th column, $k_{u+1,v+1}$ is the kernel matrix entry $u + 1$ -th row, $v + 1$ -th column, and b_q is bias for the q -th kernel. Then the process of calculating the ReLU activation function is carried out from the results of the convolution layer. Rectified Linear Unit (ReLU) is one of the activation functions used in CNN where if the input of the activation function is negative then the output changes to zero. Meanwhile, if the input of the activation function is positive, then the output is the value of the input itself. Mathematically, ReLU can be defined in Equation (10).

$$t_{i,j} = r(v_{i,j}) = \max(0, x) = \begin{cases} v_{i,j} & \text{jika } v_{i,j} \geq 0 \\ 0 & \text{jika } v_{i,j} < 0 \end{cases} \quad (10)$$

where, $t_{i,j}$ is the output result of the ReLU activation function and $v_{i,j}$ is the input pixel value from the result of the convolution layer operation. The results of the ReLU activation function are normalized using batch normalization. Batch Normalization is a normalization process for each layer in the network that is applied before or after the activation function [35]. Batch Normalization results are calculated by first calculating the average (μ_j) and variance (σ_j^2), then normalizing them. The process of calculating the average (μ_j), variance (σ_j^2), and normalization is carried out using Equations (11), (12), and (13).

$$\mu_j = \frac{1}{m} \sum_{i=1}^m t_{i,j} \quad (11)$$

$$\sigma_j^2 = \frac{1}{m} \sum_{i=1}^m (t_{i,j} - \mu_j)^2 \quad (12)$$

$$g = \hat{t}_{ij} = \frac{t_{ij} - \mu_j}{\sqrt{\sigma_j^2 + \varepsilon}} \quad (13)$$

where, μ_j s the average value of each mini batch, σ_j^2 is the variance value for each mini batch, j s the number of mini batches, m is the amount of data in a mini batch, \hat{t}_{ij} the result of normalizing input values in the i -th row and the j -th column, t_{ij} is the input matrix entry resulting from the operation of the ReLU activation function in i -th row and j -th column, and ε is the smallest constant value. Then the dimension reduction is carried out on the feature map resulting from batch normalization using maxpooling. In the decoder section, the convolution layer operation is performed, the ReLU activation function, the same batch normalization as in the encoder section. Then, the feature map dimensions are increased by using upsampling on the decoder section. The results of operations on the encoder and decoder are combined using concatenate. Then perform the calculation operation of the sigmoid activation function using Equation (14) [36].

$$s = f(g) = \frac{1}{1 + e^{-g}} \quad (14)$$

where, s is the output of the sigmoid activation function and g is the input of batch normalization results. The final stage is to calculate the loss function using binary cross entropy. binary cross-entropy is the loss function used to calculate the loss in the two-class case. Binary cross-entropy is calculated using Equation (15) [37].

$$H_p(s) = -\frac{1}{n} \sum_{i=1}^n (s_i \times \log(p(s_i)) + (1 - s_i) \times \log(1 - p(s_i))) \quad (15)$$

where, n is the predicted matrix row, s_i is the class in the classification, $p(s_i)$ is the probability value of s_i , and $H_p(s)$ is the binary cross entropy result.

2.4 PERFORMANCE EVALUATION

The success of the method proposed in this study is measured by calculating the performance evaluation. The success rate of the black hat transform method to improve image quality is measured by calculating the MSE and PSNR values. The success rate of the U-Net architecture for segmenting blood vessels in retinal images is measured by calculating the values for accuracy, sensitivity, specificity, and f1-score. The MSE and PSNR value is calculated using Equation (16) and (17) [38].

$$MSE = \frac{1}{mn} \sum_{i=0}^{m-1} \sum_{j=0}^{n-1} [I_{i,j} - N_{i,j}]^2 \quad (16)$$

$$PSNR = 20 \cdot \log_{10}(I_{max}) - 10 \cdot \log_{10}(MSE) \quad (17)$$

where, m and n are image dimensions, $I_{i,j}$ is the pixel value of the original image in the i -th row and j -th column, $N_{i,j}$ is the pixel value of the image enhancement result in the i -th row and j -th column, and I_{max} is the maximum value of the image pixel. The accuracy value is calculated to measure the accuracy of the segmentation model. The sensitivity value indicates the accuracy of the model in recognizing blood vessel features (foreground) in retinal images. The specificity value indicates the accuracy of the model in recognizing the background on the retinal image. F1-score is calculated to measure the comparison between sensitivity and specificity values. The results of the performance evaluation in this study will be compared with the results of several previous studies.

3. RESULTS AND DISCUSSION

3.1 IMAGE ENHANCEMENT

The retinal image used in this study comes from the DRIVE dataset with dimensions of 564×584 pixels. An example of the results of the image enhancement stages in the DRIVE dataset can be seen in Figure 3. Image enhancement is carried out in several stages, including changing the appearance of the BGR image to RGB, split green channel, grayscale, CLAHE, opening morphology, gamma correction, and black hat transform.

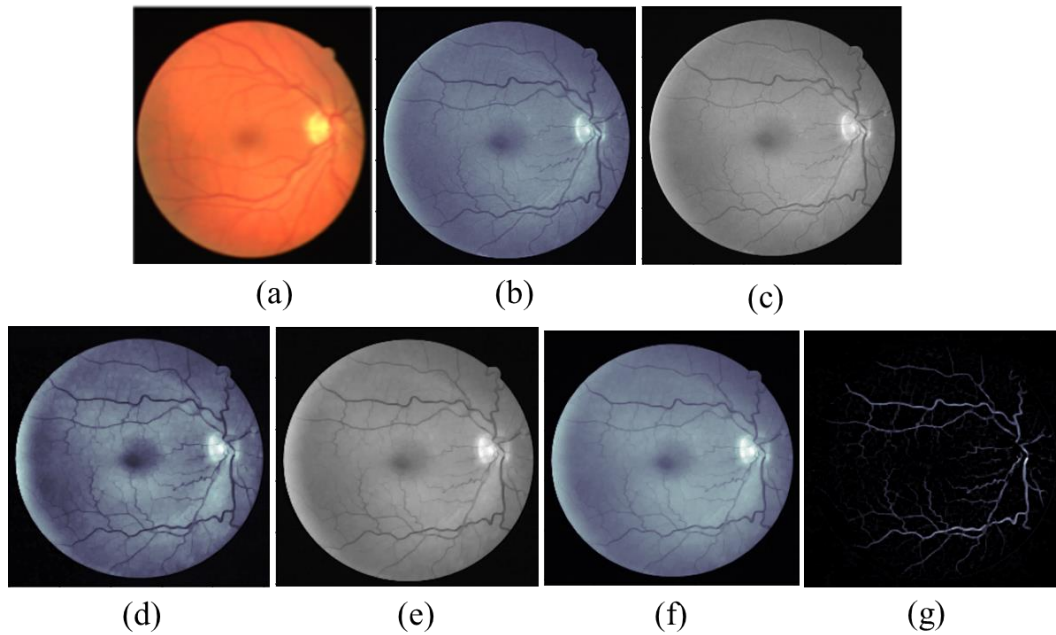


FIGURE 3. Results of the Image Enhancement Stages on the DRIVE dataset
(a) RGB Image (b) Green Channel (c) Grayscale (d) CLAHE (e) Opening Morphology (f) Gamma Correction (g) Black Hat Transform

In Figure 3, it can be seen that a split channel was carried out in the RGB image by taking the green channel. The green channel image is converted to a grayscale image. In grayscale images, quality improvement and image contrast enhancement are carried out using CLAHE, opening morphology, and gamma correction. In the final stage of image enhancement, black hat transform is used to improve the appearance of blood vessels in retinal images in detail without causing noise in the image. The results of the image enhancement stages are measured using the MSE and PSNR values. MSE is the average squared error value between the original image and the image resulting from the image enhancement stages [39]. A low MSE value means a lower error value. PSNR is a measure that shows the quality between the original image and the image resulting from the image enhancement stages. The higher the PSNR value means the better the resulting image quality [40]. The MSE and PSNR results produced at the image enhancement stage for the 20 DRIVE dataset images can be seen in Table 2.

TABLE 2.
MSE and PSNR Values from the Results of Image Enhancement Stages

No	File Name	MSE	PSNR
1	01_test.tif	0.099	90.002
2	02_test.tif	0.110	95.631
3	03_test.tif	0.111	95.233
4	04_test.tif	0.124	90.603
5	05_test.tif	0.101	99.265
6	06_test.tif	0.104	97.915
7	07_test.tif	0.109	96.234
8	08_test.tif	0.106	97.297

Cahyo Pambudi Darmo, Lucky Indra Kesuma, Dite Geovani
The Combination of Black Hat Transform and U-Net in Image Enhancement and Blood Vessel Segmentation in Retinal Images

9	09_test.tif	0.105	97.474
10	10_test.tif	0.083	90.788
11	11_test.tif	0.101	99.489
12	12_test.tif	0.105	97.764
13	13_test.tif	0.103	98.437
14	14_test.tif	0.111	95.343
15	15_test.tif	0.103	98.363
16	16_test.tif	0.113	94.626
17	17_test.tif	0.111	95.412
18	18_test.tif	0.102	98.295
19	19_test.tif	0.103	98.443
20	20_test.tif	0.095	90.219
Average		0.105	95.841

Based on Table 2, it can be seen that the average MSE and PSNR values are 0.105 and 95.841 dB, respectively. The MSE value obtained is below 0.05 and the PSNR obtained is above 90 dB. This shows that the image resulting from the image enhancement stages has good quality.

3.2. SEGMENTATION: U-NET ARCHITECTURE

At the segmentation stage, a patching technique is used to reproduce the training data where the resulting image from the black hat transform is divided into small pieces randomly. The patching technique is carried out by dividing the black hat transformed image into small pieces of 5,000 patches per image. The training data on the DRIVE dataset is available as many as 20 images so that the resulting patch is 100,000 patches with a size of 64x64 pixels. At the segmentation stage, the data is divided into two groups, namely 80% as training data and 20% as validation data. It aims to see the learning process during training. The training process is carried out as many as 50 epochs with a batch size of 8. The best weight value in the training process will be stored to be used at the testing stage. The results of the loss values and accuracy obtained in the training process can be seen in Figure 4.

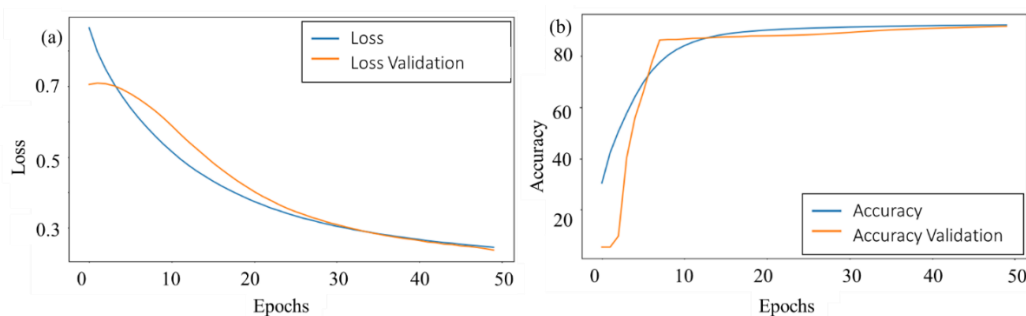


FIGURE 4. Value of (a) Loss and (b) Accuracy in the Training Process

In Figure 4(a) it can be seen that the loss value in the training process for training data and data validation continues to decrease towards a value below 0.3. In Figure 4(b) it can be seen that the accuracy value in the training process is above 80%. Accuracy values in training data and validation data continue to increase and start to stabilize from the 15th epoch. In addition to accuracy and loss values, at the training

stage recall and precision measurements are also carried out. The measured recall value shows the model's success in recognizing each feature of the image correctly, while the precision is measured to see the model's success rate in recognizing each feature correctly compared to the correctly predicted features. Graph of recall and precision values in the training process can be seen in Figure 5.

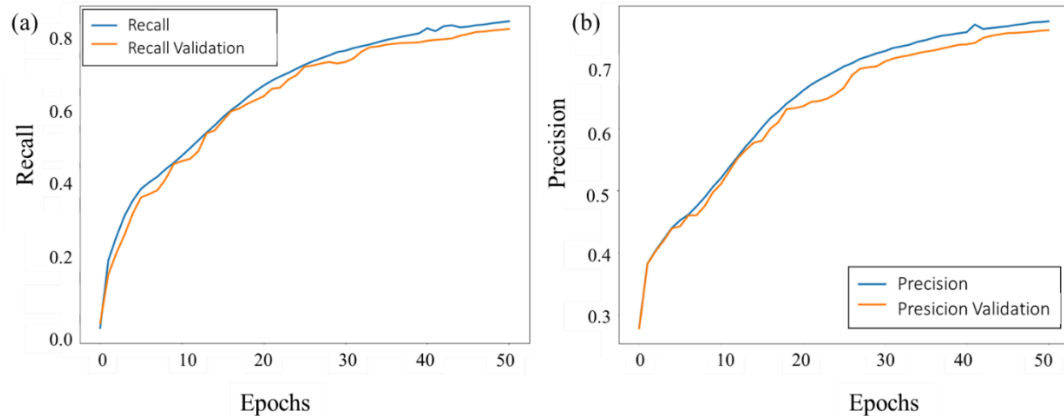


FIGURE 5. Value of (a) Recall and (b) Precision in the Training Process

In Figure 5(a) it can be seen that the recall value in the training process is above 0.8. The recall value on the training data and validation data continues to increase. In Figure 5(b) it can be seen that the precision value in the training process for training data and data validation continues to increase towards a value above 0.7. At the segmentation training stage, the f1-score measurement is also carried out. The F1-score is the average of the weighted recall and precision values. The graph of the f1-score value in the training process can be seen in Figure 6.

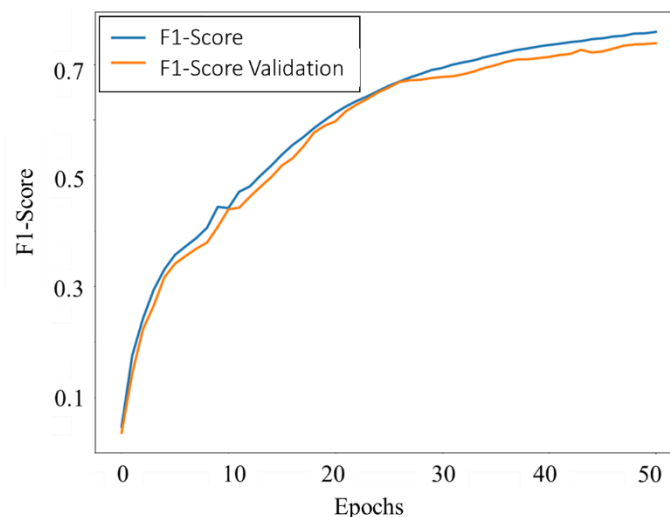



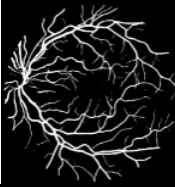



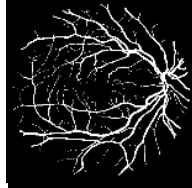
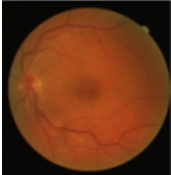
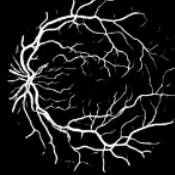
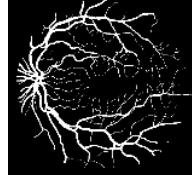
FIGURE 6. F1-Score Value in the Training Process

In Figure 6 it can be seen that the f1-score value on the training data and data validation training process continues to increase in each epoch. The f1-score value continues to increase and reaches a value above 0.7. After the training phase, a testing phase is carried out to test the model that has been trained with training data. The

Cahyo Pambudi Darmo, Lucky Indra Kesuma, Dite Geovani
The Combination of Black Hat Transform and U-Net in Image Enhancement and
Blood Vessel Segmentation in Retinal Images

testing phase is carried out using data that has not been studied by the model, namely test data on the DRIVE dataset to segment blood vessels on retinal images. Comparison of the display of prediction results of blood vessel segmentation on retinal images with ground truth can be seen in Table 3.

TABLE 3.
 Comparison of Segmentation Prediction Results and Ground Truth

No.	File Name	Original Image	Prediction Result	Ground Truth
1	01_test.tif			
2	02_test.tif			
3	03_test.tif			

Based on Table 3, it can be seen that the display of the predicted results matches the appearance of the ground truth image. This shows that the model is able to accurately recognize blood vessel features in retinal images. At the testing stage, the RMSE value is also measured. The RMSE value shows that the difference between the predicted value and the actual value has a small error or error. The graph of the RMSE value in the training process can be seen in Figure 7.

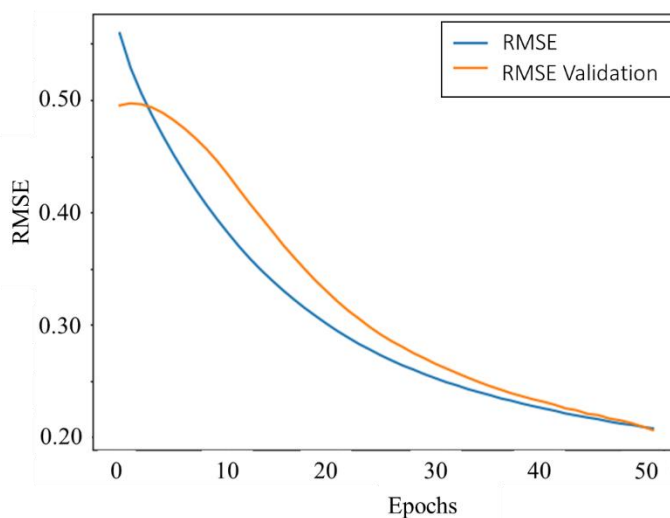


FIGURE 7. RMSE Value in the Testing Process

In Figure 7, it can be seen that the RMSE value on the training data and data validation training process is very good. The RMSE value obtained is close to 0.2 and continues to decrease at each epoch. The smaller the RMSE value, the smaller the errors that occur between the prediction results and the ground truth. At the testing stage, performance evaluation is carried out by calculating the accuracy, sensitivity, specificity, and f1-score values. The graph of the results for accuracy, sensitivity, specificity, and f1-score can be seen in Figure 8.

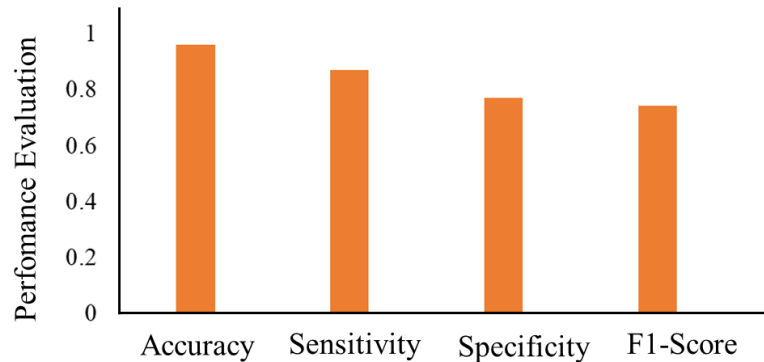


FIGURE 8. Graph of Model Performance Evaluation

In Figure 8, it can be seen that at the testing stage the accuracy value is above 0.95 and the sensitivity is above the value 0.85. The specificity value and f1-score at the testing stage are above 0.8. This shows that the model is able to accurately recognize the features of blood vessels in retinal images. Then, a comparison was made between the results obtained in this study and previous research. Comparison of the results of blood vessel segmentation in the DRIVE dataset using the U-Net architecture with previous studies can be seen in Table 4.

TABLE 4.
Comparison of Performance Evaluation Results with Other Studies

No.	Methods	Accuracy	Sensitivity	Specificity	F1-Score
1	Fully Connected [12]	0.94	0.77	-	-
2	Res-Net [41]	-	0.79	0.98	0.86
3	SVM [42]	0.94	0.51	0.99	-
4	Com U-Net [43]	0.95	0.80	0.98	0.79
5	U-Net (Proposed Methods)	0.96	0.87	0.82	0.80

Based on table 4, it can be seen that this study has the highest accuracy and sensitivity values compared to other studies. this shows that the model in this study is accurate in segmenting blood vessels in retinal images and is able to recognize blood vessel features in retinal images very well. The study conducted by Escorcía [42] had the highest specificity value compared to other studies with a value above 0.95, but had the lowest sensitivity value with a value below 0.55 and did not measure an f1-score. research conducted by Li [41] has the highest f1-score, but does not measure accuracy.

4. CONCLUSION

Based on the results and discussion, the results of image enhancement using black hat transform have very good MSE and PSNR values. The MSE value obtained is below 0.05, this indicates that the difference between the pixel values in the image enhancement results and the original image is very small. The PSNR value obtained is above 90 dB. This shows that the image resulting from the image enhancement stages has good quality. The results of blood vessel segmentation on retinal images also have very good value. This study has an accuracy value above 0.95 and a sensitivity value above 0.85. The specificity value and f1-score of this study were above 0.8. This shows that the model is able to accurately recognize the features of blood vessels in retinal images.

REFERENCES

- [1] B. W. Asril, M. Maison, and A. Yudertha, "Analisis Performa Algoritma Segmentasi Pembuluh Darah pada Citra Fundus Retina," *J. Edukasi dan Penelit. Inform.*, vol. 5, no. 3, p. 272, 2019.
- [2] R. A. Aras, T. Lestari, H. A. Nugroho, and I. Ardiyanto, "Segmentation of Retinal Blood Vessels for Detection of Diabetic Retinopathy: A review," *Commun. Sci. Technol.*, vol. 1, no. 1, pp. 33–41, 2016.
- [3] K. Radhika and S. Vinay, "Prediction of Diabetic Retinopathy Using InceptionV3 Model," *Int. J. Adv. Eng. Manag.*, vol. 4, no. 7, pp. 1327–1331, 2022.
- [4] W. Cahyaningrum, R. C. Wihandika, and A. W. Widodo, "Segmentasi Pembuluh Darah pada Citra Retina Menggunakan Algoritme Multi-Scale Line Operator dan Preprocessing Data dengan K-Means," *J. Pengemb. Teknol. Inf. dan Ilmu Komput.*, vol. 2, no. 6, pp. 2353–2363, 2018.
- [5] A. Desiani *et al.*, "Combination Contrast Stretching and Adaptive Thresholding for Retinal Blood Vessel Image," *Manajemen, Tek. Inform. dan Rekayasa Komput.*, vol. 22, no. 1, pp. 1–12, 2021.
- [6] X. Liu, S. Wang, Y. Zhang, D. Liu, and W. Hu, "Automatic Fluid Segmentation in Retinal Optical Coherence Tomography Images using Attention Based Deep Learning," *Neurocomputing*, vol. 452, pp. 576–591, 2021.
- [7] R. Benenson, S. Popov, and V. Ferrari, "Large-Scale Interactive Object Segmentation with Human Annotators," in *Proceedings of the IEEE Computer Society Conference on Computer Vision and Pattern Recognition*, 2019, vol. 2019-June, pp. 11692–11701.
- [8] H. A. Khan, W. Jue, M. Mushtaq, and M. U. Mushtaq, "Brain Tumor Classification in MRI Image Using Convolutional Neural Network," *Math. Biosci. Eng.*, vol. 17, no. 5, pp. 6203–6216, 2020.
- [9] A. A. Pravitasari *et al.*, "UNet-VGG16 with Transfer Learning for MRI-Based Brain Tumor Segmentation," *Telkomnika (Telecommunication Comput. Electron. Control.*, vol. 18, no. 3, pp. 1310–1318, 2020.
- [10] N. Navab, J. Hornegger, W. Wells, and A. F. Frangi, *Medical Image Computing and Computer Assisted Intervention*. 2015.
- [11] V. Sathananthavathi and G. Indumathi, "Encoder Enhanced Atrous (EEA) Unet architecture for Retinal Blood vessel segmentation," *Cogn. Syst. Res.*, vol. 67,

- pp. 84–95, 2021.
- [12] H. Fu, Y. Xu, D. W. K. Wong, and J. Liu, “Retinal Vessel Segmentation via Deep Learning Network and Fully-Connected Conditional Random Fields,” in *Proceedings - International Symposium on Biomedical Imaging*, 2016, vol. 2016-June, pp. 698–701.
- [13] G. M. Venkatesh, Y. G. Naresh, S. Little, and N. E. O’Connor, *A deep residual architecture for skin lesion segmentation*, vol. 11041 LNCS. Springer International Publishing, 2018.
- [14] A. Saood and I. Hatem, “COVID-19 lung CT image segmentation using deep learning methods: U-Net versus SegNet,” *BMC Med. Imaging*, vol. 21, no. 1, pp. 1–10, 2021.
- [15] Z. Zainudin, S. M. Shamsuddin, and S. Hasan, *Deep Layer CNN Architecture for Breast Cancer Histopathology Image Detection*, vol. 921. Springer International Publishing, 2020.
- [16] A. Desiani, D. A. Zayanti, R. Primartha, F. Efriliyanti, and N. A. C. Andriani, “Variasi Thresholding untuk Segmentasi Pembuluh Darah Citra Retina,” *J. Edukasi dan Penelit. Inform.*, vol. 7, no. 2, p. 255, 2021.
- [17] V. Bhayyu and N. Elvira, “Perbandingan Antara Metode Otsu Thresholding dan Multilevel Thresholding untuk Segmentasi Pembuluh Darah Retina,” in *Annual Research Seminar (ARS)*, 2019, vol. 4, no. 1, pp. 978–979.
- [18] V. Nurdinawati, A. Hendryani, and T. Barasabha, “Segmentasi Citra Pembuluh Darah Retina Menggunakan Operasi Morfologi Iteratif,” *J. Tek. Elektro*, vol. 13, no. 1, pp. 18–24, 2021.
- [19] N. Singh, L. Kaur, and K. Singh, “Histogram Equalization Techniques for Enhancement of Low Radiance Retinal Images for Early Detection of Diabetic Retinopathy,” *Eng. Sci. Technol. an Int. J.*, vol. 22, no. 3, pp. 736–745, 2019.
- [20] A. H. Khan, D. N. F. A. Iskandar, J. F. Al-Asad, and S. El-Nakla, “Classification of Skin Lesion with Hair and Artifacts Removal using Black-hat Morphology and Total Variation,” *Int. J. Comput. Digit. Syst.*, vol. 10, no. 1, 2021.
- [21] J. Jayanthi, E. L. Lydia, N. Krishnaraj, T. Jayasankar, R. L. Babu, and R. A. Suji, “An Effective Deep Learning Features based Integrated Framework for Iris Detection and Recognition,” *J. Ambient Intell. Humaniz. Comput.*, vol. 12, no. 3, pp. 3271–3281, 2021.
- [22] I. Nizovtseva *et al.*, “Assessing The Mass Transfer Coefficient in Jet Bioreactors with Classical Computer Vision Methods and Neural Networks Algorithms,” *Algorithms*, vol. 16, no. 3, p. 125, 2023.
- [23] W. Wang, W. Wang, and Z. Hu, “Segmenting Retinal Vessels with Revised Top-Bottom-Hat Transformation and Flattening of Minimum Circumscribed Ellipse,” *Med. Biol. Eng. Comput.*, vol. 57, no. 7, pp. 1481–1496, 2019.
- [24] R. Kushol, M. H. Kabir, M. S. Salekin, and A. B. M. Ashikur Rahman, “Contrast Enhancement by Top-hat and Bottom-hat Transform with Optimal Structuring Element: Application to Retinal Vessel Segmentation,” *Lect. Notes Comput. Sci. (including Subser. Lect. Notes Artif. Intell. Lect. Notes Bioinformatics)*, vol. 10317 LNCS, pp. 533–540, 2017.
- [25] B. Mughal, M. Sharif, N. Muhammad, and T. Saba, “A Novel Classification Scheme to Decline The Mortality Rate Among Women due to Breast Tumor,” *Microsc. Res. Tech.*, vol. 81, no. 2, pp. 171–180, 2018.

Cahyo Pambudi Darmo, Lucky Indra Kesuma, Dite Geovani
The Combination of Black Hat Transform and U-Net in Image Enhancement and
Blood Vessel Segmentation in Retinal Images

- [26] A. K. Yadav, "Detection of Hard Exudates in Retinopathy Images," *Adv. Distrib. C. Artif. Intell.*, vol. 8, no. 4, 2019.
- [27] B. Kim, R. O. Serfa Juan, D. E. Lee, and Z. Chen, "Importance of Image Enhancement and CDF for Fault Assessment of Photovoltaic Module using IR Thermal Image," *Appl. Sci.*, vol. 11, no. 18, 2021.
- [28] L. M. Chu, C. W. Lee, H. C. Hsu, C. Y. Liu, T. H. Li, and S. C. Hsiung, "Development of Oil Film Thickness Measurement Software Using Optical Interferometry," *Sensors Mater.*, vol. 34, no. 8, pp. 3229–3239, 2022.
- [29] J. Dash and N. Bhoi, "Retinal Blood Vessel Segmentation using Otsu Thresholding with Principal Component Analysis," *Proc. 2nd Int. Conf. Inven. Syst. Control. ICISC 2018*, no. Icisc, pp. 933–937, 2018.
- [30] D. Rahmawati, R. Alfita, M. Ulum, and D. Murdianto, "Tobacco Farming Mapping To Determine The Number Of Plants Using Contour Detection Method," in *E3S Web of Conferences*, 2021, vol. 328, pp. 6–11.
- [31] R. Kosasih and A. Fahrurrozi, "Vehicle Detection Using Principal Component Analysis," *J. Ilm. Komputasi*, vol. 19, no. 2, pp. 155–160, 2020.
- [32] S. Dash and M. R. Senapati, "Enhancing Detection of Retinal Blood Vessels by Combined Approach of DWT, Tyler Coxe and Gamma correction," *Biomed. Signal Process. Control*, vol. 57, p. 101740, 2020.
- [33] A. Acharya and A. V. Giri, "Contrast Improvement using Local Gamma Correction," in *2020 6th International Conference on Advanced Computing and Communication Systems, ICACCS 2020*, 2020, pp. 110–114.
- [34] T. Guo, J. Dong, H. Li, and Y. Gao, "Simple Convolutional Neural Network on Image Classification," in *International Conference on Big Data Analysis*, 2017, pp. 721–724.
- [35] S. Ioffe and C. Szegedy, "Batch Normalization: Accelerating Deep Network Training by Reducing Internal Covariate Shift," *Journal. Pract.*, vol. 10, no. 6, pp. 730–743, 2016.
- [36] S. Ngah and R. A. Bakar, "Sigmoid Function Implementation using The Unequal Segmentation of Differential Lookup Table and Second Order Nonlinear Function," *Telecommun. Electron. Comput. Eng.*, vol. 9, no. 2–8, pp. 103–108, 2017.
- [37] R. Yu, Y. Wang, Z. Zou, and L. Wang, "Convolutional Neural Networks with Refined Loss Functions for The Real-time Crash Risk Analysis," *Transp. Res. Part C Emerg. Technol.*, vol. 119, no. April, p. 102740, 2020.
- [38] A. Kuznetsov, O. Smirnov, L. Gorbacheva, and V. Babenko, "Hiding Data In Images using A Pseudo-Random Sequence," in *CEUR Workshop Proceedings*, 2020, vol. 2608, pp. 646–660.
- [39] U. Sara, M. Akter, and M. S. Uddin, "Image Quality Assessment through FSIM, SSIM, MSE and PSNR—A Comparative Study," *J. Comput. Commun.*, vol. 07, no. 03, pp. 8–18, 2019.
- [40] P. Kandhway and A. K. Bhandari, *An Optimal Adaptive Thresholding based Sub-histogram Equalization for Brightness Preserving Image Contrast Enhancement*, vol. 30, no. 4. Springer US, 2019.
- [41] D. Li, D. A. Dharmawan, B. P. Ng, and S. Rahardja, "Residual U-Net for Retinal Vessel Segmentation," in *2019 IEEE International Conference on Image Processing (ICIP)*, 2019, pp. 1425–1429.
- [42] J. Escorcia-Gutierrez *et al.*, "A Feature Selection Strategy to Optimize Retinal Vasculature Segmentation," *Comput. Mater. Contin.*, vol. 70, no. 2, pp. 2971–



2989, 2022.

- [43] C. Wang, Z. Zhao, and Y. Yu, “Fine Retinal Vessel Segmentation by Combining Nest U-Net and Patch-Learning,” *Soft Comput.*, vol. 25, no. 7, pp. 5519–5532, 2021.